Microscopic treatment of the angular dependence of surface induced optical anisotropy

C. M. J. Wijers and G. P. M. Poppe
Twente University, P. O. Box 217, 7500 AE Enschede, The Netherlands
(Received 13 September 1991; revised manuscript received 26 February 1992)

The angular dependency of surface induced optical anisotropy (SIOA) has been calculated by means of the discrete dipole approach. Within the basic assumptions of this approach, exact results (full incorporation of local-field effects and retardation) have been obtained for the semi-infinite problem using the double-cell method. This method allows for an independent treatment of bulk and surface. For off-normal incidence, the microscopic behavior of the system has been investigated. Near the Brewster angle, the absolute value of the microscopic p-type response is larger than the s-type response. In general, the SIOA decreases for increasing angles of incidence. Only near Brewster's angle the relative p-type anisotropic reflectance difference increases dramatically, but under experimentally very unstable conditions. Further, the macroscopic anisotropic response, dR_s/R_0, dR_p/R_0, $\delta\Psi$, and $\delta\Delta$, has been calculated as a function of photon energy for three angles of incidence, 60°, 70°, and 80°, and for the (110) surfaces of three popular semiconductors, Si, GaP, and GaAs, respectively.

I. INTRODUCTION

Although the anisotropic optical response of surfaces of cubic materials has been reported by Furtak and Lynch[1] for Ag(110), the observation of optical anisotropy at the Si(111)-2×1 surface by Chiaradia *et al.*,[2] where the unreconstructed situation should behave isotropically, has generated large interest. These optical experiments have played a key role in establishing the Pandey chain model[3] as the reconstruction of the Si(111)-2×1 surface. They showed the potential of surface optics, optics sensitive to the outermost monolayers of the surface, for use as an analytical tool. Surface anisotropy, as displayed by the Si(111)-2×1 surface, and other anisotropic surfaces of cubic crystals, is a special branch of surface optics and will collectively be referred to by us as surface induced optical anisotropy (SIOA). The classical Fresnel approach will not predict SIOA. Early theoretical work in the field of surface optics has been performed by Bagchi and co-workers[4–6] and Mochán and coworkers.[7,8] The general basis for the theoretical description of this kind of optical response problem from the continuum point of view has been laid by Del Sole and Fiorino.[9] In a number of subsequent papers, this theoretical description has been used to calculate the anisotropic reflectance difference spectra of Si(111)-2×1.[10–12] Until recently, the determination of surface reconstruction was the prime interest in surface optics. The focus has now changed to an improved understanding of surface optics, itself. We may consider as a turning point the studies of SIOA at (110) surfaces by Mochán and Barrera,[8] who incorporated the influence of classical local-field effects in anisotropic reflection from unreconstructed (110) surfaces and by Aspnes,[13] who measured the anisotropic reflection of Si and Ge (110) surfaces in a dry nitrogen atmosphere and discussed the theoretical implications of those observations. Parallel to the experimental work on the anisotropic surfaces of elementary semiconductors, the anisotropic reflectance difference spectra for (110) surfaces of III-V compounds have been measured by Selci *et al.*[14] and by Berkovits *et al.*[15–17] Important work has been done on the (110) surface of GaP, the only III-V compound having an isolated (110) surface state inside the energy gap, and the (001) GaAs surface.[18] This limited amount of experimental information was later used extensively by theoreticians who wanted a fundamental understanding of the behavior of electromagnetic waves at the very moment they enter a solid surface and affect, in particular, the few outermost atomic layers. These few examples show that anisotropic reflectance spectroscopy still contains fundamental problems regarding the understanding of the solid-matter interaction. This makes it even more surprising that all of this work, both theoretical and experimental, has been obtained for perpendicular incidence only. It is the aim of this paper to focus upon the angular dependence of SIOA from a theoretical point of view. Previously, we have shown that discrete dipole theory reveals some major aspects of the SIOA problem, notably the role of the wiggling zone,[19–21] the influence of large surface reconstructions,[22] and some preliminary investigations about the angular dependency of SIOA (Ref. 23) (Ref. 23 will hereafter be referred to as I). We will give here a full derivation of the double-cell (DC) method, which allows for direct calculation of the SIOA of semi-infinite systems. We will verify the validity of this method by comparing the results of this method and of the preceding two-slab (TS) method.[23] Using the DC method, the microscopic angular-dependent behavior will be studied. Finally, for the three semiconductors Si, GaP, and GaAs, the SIOA caused by their (110) surface will be calculated as a function of energy for some angles, being in the range of common ellipsometers. The data obtained in this way can be used to interpret anisotropic spectroscopic ellipsometric experiments.

II. DISCRETE DIPOLE THEORY OF ANGULAR DEPENDENT REFLECTION

We will treat discrete dipole theory only for systems obeying parallel translational symmetry. In previous publications, we have treated the key elements that build the basics of such a theory, these elements being the principles of induction, superposition and parallel translational symmetry, and the Hertz potential formalism.[23] We will start by treating the geometry of an arbitrary parallel translational system. Next we will explain the general strategy to obtain reflection-transmission by means of the discrete dipole approach. This requires, first, the solution of the interaction equations from which the individual dipole strengths will be obtained and, next, use of those dipole strengths in the expression for the propagator to obtain the remote response. We will start with some useful conventions. Any vector $\mathbf{u}$ can be decomposed into components parallel and normal to the lattice planes according to

$$\mathbf{u}=(\mathbf{u}_{\parallel},u_z)=(u_x,u_y,u_z)\ . \tag{1}$$

For the same vector one defines the reflected counterpart $\underline{\mathbf{u}}$ as

$$\underline{\mathbf{u}}=(\mathbf{u}_{\parallel},-u_z)\ . \tag{2}$$

Finally, we need some conventions with respect to dot products and direct products of two vectors $\mathbf{u}$ and $\mathbf{v}$, where sometimes an upper index T is advantageous:

$$\begin{aligned}&\mathbf{u}^T\mathbf{v}=\mathbf{u}\cdot\mathbf{v}=\mathbf{uv}\ ,\\ &[\mathbf{uv}^T]_{ij}=u_iv_j\quad(i,j=x,y,z)\ .\end{aligned} \tag{3}$$

Mostly, the dot product will be used by us without upper index or dot. One place where the upper T convention is useful is in the following contraction rule:

$$\mathbf{u}(\mathbf{v}^T\mathbf{w})=(\mathbf{uv}^T)\mathbf{w}\ , \tag{4}$$

which turns out to be very useful in the full version of discrete dipole theory.

A. Description of the configuration

The configuration of a reflection setup is shown in Fig. 1. The crystalline bulk or slab is located in the upper half space and the electromagnetic beam impinges from the lower half space. The derivation of the theory to be treated in this paper will be general, but all specific cases studied in detail will concern simple fcc-type dipole lattices in the (110) orientation. Hence, these lattice planes of dipoles have to be spanned by the lateral basis vectors $\mathbf{s}_1$ and $\mathbf{s}_2$:

$$\begin{aligned}&\mathbf{s}_1=(a,0,0)\ ,\\ &\mathbf{s}_2=(\alpha a,\beta a,0)\ .\end{aligned} \tag{5}$$

a is the normalization length, $a^c=\sqrt{2}a$ (a^c is the lattice constant of the conventional bulk unit cell), $\alpha=0$, and $\beta=\sqrt{2}$. By convention, $\mathbf{s}_1$ will be the shorter basis vector. The lattice planes are mutually separated by multiples of the interlayer spacing $\mathbf{d}$:

$$\mathbf{d}=\tfrac{1}{2}(1,\sqrt{2},1)a\ . \tag{6}$$

The $\hat{\mathbf{x}}$ axis is in the direction of $\mathbf{s}_1$, the crystallographic $(1\bar{1}0)$ direction. The angle between the plane of incidence and $\hat{\mathbf{x}}$ defines the anisotropic azimuth angle Ω, counterclockwise being positive. The incoming light beam will be defined as

$$\mathbf{E}(r,t)=E_0\hat{\mathbf{e}}\exp(i[\mathbf{kr}-\omega t])\ , \tag{7}$$

where E_0 represents the (complex) amplitude and $\hat{\mathbf{e}}$ the direction of polarization (carets will indicate unit vectors). In all that follows, the time dependence has been eliminated. For angular dependency, the directions $\hat{\mathbf{s}}$ and $\hat{\mathbf{p}}$ (the generic symbol $\hat{\mathbf{t}}$ will refer to both) have to be defined precisely. In our calculations we have used the following definitions:

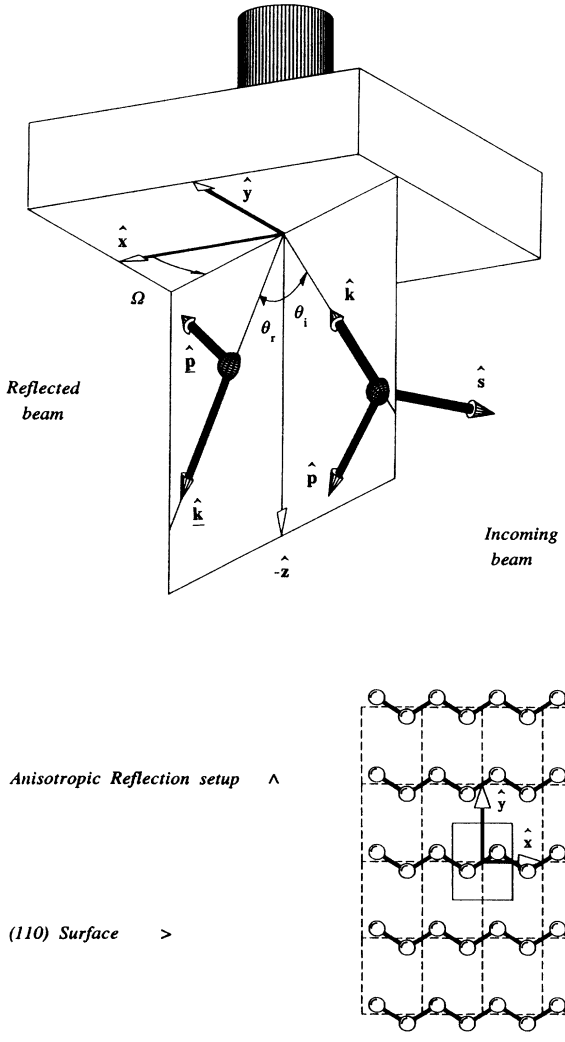

FIG. 1. Configuration of an anisotropic reflection setup. Ω, anisotropic azimuth angle; $\hat{\mathbf{s}}$, $\hat{\mathbf{p}}$, polarization directions; $\hat{\mathbf{k}}$, $\underline{\hat{\mathbf{k}}}$, incoming and reflected wave-vector direction, respectively; θ_i, θ_r, angle of incidence and reflection, respectively.

$$\hat{\mathbf{s}}=\mathbf{k}\times\hat{\mathbf{z}}/|\mathbf{k}\times\hat{\mathbf{z}}| \ , \qquad \hat{\mathbf{p}}=\hat{\mathbf{k}}\times\hat{\mathbf{s}} \ . \tag{8}$$

For reflected p-polarized light, our choice for $\hat{\mathbf{t}}$ will be $\hat{\mathbf{p}}$, for mathematical consistency (Fig. 1). Experimentalists prefer the assignment $\hat{\mathbf{t}}=-\hat{\mathbf{p}}$, according to the Muller-Nebraska convention.

B. Interaction equations (general)

1. Calculation of dipole strengths

Reference 24 gives the procedure used for the calculation of the polarizability tensor $\overleftrightarrow{\alpha}_i$ and a summary of it, including results, will be given at the beginning of Sec. III. The polarizability normalization factor is defined as $\alpha_0=4\pi\epsilon_0 a^3$. Parallel translational symmetry gives rise to lattice sums and transfer tensors, whose classification can be found in Refs. 19 and 25. Here we will add the derivation of the interplanar far lattice sums (Appendix A) and transfer tensors. As a result of parallel translational symmetry, a single dipole $\mathbf{p}_j$ will control the entire electromagnetic response of a single lattice plane of dipoles j, and in the rest of this paper we will only consider those characteristic dipoles $\mathbf{p}_j$. The transfer tensors $\mathbf{f}_j(\mathbf{r})$ give the electric field $\mathbf{E}$ caused at site $\mathbf{r}$ by a plane of dipoles j:

$$\mathbf{E}_j(\mathbf{r})=\alpha_0^{-1}\overleftrightarrow{\mathbf{f}}_j(\mathbf{r})\mathbf{p}_j \ . \tag{9}$$

As defined in (9), the transfer tensors become dimensionless. The interaction equations of dipole theory for systems with parallel translational symmetry are[20,24]

$$\mathbf{p}_i=\overleftrightarrow{\alpha}_i\left[\mathbf{E}(\mathbf{r}_i)+\alpha_0^{-1}\sum_j\overleftrightarrow{\mathbf{f}}_{ij}\mathbf{p}_j\right] , \tag{10a}$$

$$\overleftrightarrow{\mathbf{f}}_{ij}=\overleftrightarrow{\mathbf{f}}_j(\mathbf{r}_i) \ . \tag{10b}$$

The site $\mathbf{r}_i$ represents the location of the ith characteristic dipole. The anisotropic azimuth Ω controls those equations implicitly through the transfer tensors $\mathbf{f}_{ij}$. Usually the diagonal tensors $\mathbf{f}_{ii}$ become referred to as $\mathbf{c}$. The interaction matrix $\mathbb{M}$ obeys the usual definition:

$$\|\mathbb{M}\||\mathbf{p}_i|=|\mathbf{E}(\mathbf{r}_i)| \ , \tag{11a}$$

$$\overleftrightarrow{\mathbb{M}}_{ij}=\overleftrightarrow{\alpha}_i^{-1}\delta_{ij}-\alpha_0^{-1}\overleftrightarrow{\mathbf{f}}_{ij} \ . \tag{11b}$$

The factorization of the interaction equations, for the cases studied in this paper and already used in I, will be considered in detail in Sec. II D.

2. Semi-infinite systems: double-cell method

Equations (10) and (11) cannot be solved as they are for semi-infinite systems. This requires a modification via the DC method. The DC method subdivides the semi-infinite system into a bulk region and a surface layer. The bulk region will be constructed by adding repeatedly, in the z direction over a distance d_B, a stack of N_B dipole planes on top of the surface layer. The N_B characteristic dipoles of this stack make up the bulk unit cell. An arbitrary characteristic dipole v of the Vth bulk unit cell is located at

$$\mathbf{r}_{vV}=\mathbf{r}_v^B+(d_S+Vd_B)\hat{\mathbf{z}} \ . \tag{12}$$

Index V starts from 0. For the characteristic dipoles of the bulk unit cell, $z_1^B=0$ should hold for the first and $z_v^B\geq 0$ for all others. These conditions implicitly define d_S, which should be preferably larger than the largest z coordinate of the surface layer. Not all crystalline substrates can be described by (12), but the number of exceptions is negligible in practice. The surface layer itself will be subdivided into a free surface layer and a bulklike surface layer (matching layer). The first plane of the surface layer has $z_1=0$ and for arbitrary surface plane i, $z_i\geq 0$ has to hold. The free surface layer consists of dipole planes, whose characteristic dipoles can further be chosen arbitrarily. The bulklike layer consists of bulk planes according to (12), but with $V<0$. The N_S characteristic dipoles of the surface layer build the surface unit cell. For a semi-infinite system obeying this geometry the interaction equations (10) have to be solved. We investigate separately an arbitrary dipole located in the *surface layer* and one located in the *bulk region*. Starting with the bulk, we need first some definitions. From Appendix A, the quantity κ_{pq} will be repeated ($\mathbf{k}_0$ replaced by $\mathbf{k}$):

$$\mathbf{k}_m=(\mathbf{k}_\parallel,q_m) \ , \tag{13a}$$

$$\mathbf{k}_{pq}=(\mathbf{k}_\parallel+\mathbf{g}_{pq}^\parallel,\kappa_{pq}) \ , \tag{13b}$$

$$\kappa_{pq}=\sqrt{k^2-(\mathbf{k}_\parallel+\mathbf{g}_{pq}^\parallel)^2} \ . \tag{13c}$$

Here $\mathbf{g}_{pq}^\parallel$ is the surface reciprocal-lattice vector (Appendix A). These definitions, which follow directly from (A15) and (A16), are necessary for the following expressions for the transfer tensors. We introduce the transverse projectors $\mathbf{d}_{pq}$ as

$$\overleftrightarrow{\mathbf{d}}_{pq}=\overleftrightarrow{\mathbf{d}}(\mathbf{k}_{pq})=\frac{2\pi i a^3}{|\mathbf{s}_1\times\mathbf{s}_2|}\frac{k^2\overleftrightarrow{\mathbf{1}}-\mathbf{k}_{pq}\mathbf{k}_{pq}^T}{\kappa_{pq}} \ . \tag{14}$$

For positive $(z-z_j)$ the transfer tensor becomes

$$\overleftrightarrow{\mathbf{f}}_j(\mathbf{r})=\sum_{pq}^{\infty}\exp[i\mathbf{k}_{pq}\cdot(\mathbf{r}-\mathbf{r}_j)]\overleftrightarrow{\mathbf{d}}_{pq} \tag{15}$$

and for negative $(z-z_j)$

$$\overleftrightarrow{\mathbf{f}}_j(\mathbf{r})=\sum_{pq}^{\infty}\exp[i\underline{\mathbf{k}}_{pq}\cdot(\mathbf{r}-\mathbf{r}_j)]\overleftrightarrow{\underline{\mathbf{d}}}_{pq} \ , \tag{16a}$$

$$\overleftrightarrow{\underline{\mathbf{d}}}_{pq}=\overleftrightarrow{\mathbf{d}}(\underline{\mathbf{k}}_{pq}) \ , \tag{16b}$$

has to be used. Definitions (13)–(16) avoid the pileup of variables, which makes this part of discrete dipole theory so inaccessible.[26] *For an arbitrary dipole* $\mathbf{p}_{vV}$ *belonging to the bulk region* the interaction equations (10) become

$$\mathbf{p}_{vV}=\overleftrightarrow{\alpha}_v\left[E_0\hat{\mathbf{e}}e^{i\mathbf{k}\mathbf{r}_{vV}}+\alpha_0^{-1}\left[\sum_{j=1}^{N_S}\overleftrightarrow{\mathbf{f}}_{vVj}\mathbf{p}_j\right]+\alpha_0^{-1}\sum_{w=1}^{N_B}\left[\sum_{w=0}^{V-1}\overleftrightarrow{\mathbf{f}}_{vVwW}\mathbf{p}_{wW}+\overleftrightarrow{\mathbf{f}}_{vVwV}\mathbf{p}_{wV}+\sum_{W=V+1}^{\infty}\overleftrightarrow{\mathbf{f}}_{vVwW}\mathbf{p}_{wW}\right]\right]. \quad (17)$$

These interaction equations for a crystalline bulk can be solved by means of a normal-mode decomposition, as done originally by Litzman[26] (also, Grindlay[27] and Mochán and Barrera[28] have made comparable use of normal modes). First, we postulate the following ansatz for the bulk dipole strengths:

$$\mathbf{p}_{vV}=\sum_{m=1}^{M}\nu_m\mathbf{u}_{mv}e^{iq_mVd_B}. \quad (18)$$

The dipole strength of site vV is $\mathbf{p}_{vV}$. q_m represents the normal-mode wave numbers, $\mathbf{u}_{mv}$ refers to the normal-mode eigenvectors, which affect all dipoles of the bulk unit cell through the index v, and ν_m is the normal-mode strength, being the free variables of the normal-mode decomposition. Working from (17) by means of (18), (15), and (16) and performing the summations over the bulk unit-cell index V yields

$$-\alpha_0^{-1}\sum_{m=1}^{M}\nu_m\sum_{w=1}^{N_B}\sum_{pq}^{\infty}\left[\frac{e^{i\mathbf{k}_{pq}(\mathbf{r}_v^B-\mathbf{r}_w^B)}\overleftrightarrow{\mathbf{d}}_{pq}}{1-\exp(i[q_m-\kappa_{pq}]d_B)}\right]\mathbf{u}_{mw}e^{i\kappa_{pq}Vd_B}+\sum_{m=1}^{M}\nu_m\left[\sum_{w=1}^{N_B}\overleftrightarrow{\mathbb{A}}_{vw}\mathbf{u}_{mw}\right]e^{iq_mVd_B}$$
$$-\alpha_0^{-1}\sum_{j=1}^{N_S}\sum_{pq}^{\infty}e^{i[\mathbf{k}_{pq}(\mathbf{r}_v^B-\mathbf{r}_j)+\kappa_{pq}d_S]}\overleftrightarrow{\mathbf{d}}_{pq}\mathbf{p}_je^{i\kappa_{pq}Vd_B}=E_0\hat{\mathbf{e}}e^{i\mathbf{k}\mathbf{r}_v^B}e^{ik_z(Vd_B+d_S)}, \quad (19)$$

where the secular matrix $\mathbb{A}(\mathbf{k}_m)$ becomes defined through its tensorial elements

$$\overleftrightarrow{\mathbb{A}}_{vw}=\overleftrightarrow{\alpha}_v^{-1}\delta_{vw}-\alpha_0^{-1}\overleftrightarrow{\mathbf{f}}_{vw}+\alpha_0^{-1}\sum_{pq}^{\infty}\left[\frac{e^{i\mathbf{k}_{pq}(\mathbf{r}_v^B-\mathbf{r}_W^B)}\overleftrightarrow{\mathbf{d}}_{pq}}{1-\exp(i[q_m-\kappa_{pq}]d_B)}+\frac{e^{i\mathbf{k}_{pq}(\mathbf{r}_v^B-\mathbf{r}_w^B)}\overleftrightarrow{\mathbf{d}}_{pq}}{1-\exp(-i[q_m+\kappa_{pq}]d_B)}\right]. \quad (20)$$

The following step in the derivation is the proper interpretation of, in particular, Eq. (19). One has to consider simultaneously all equations of type (19) obtained for the N_B values of v. This yields mathematically a composite vector equation, where the composite vector consists of N_B usual three vectors. Next, this composite equation (19) has to hold for any value of V. So, all coefficients belonging to corresponding phase factors in (19) should be equal left and right. This argument is equivalent to Litzman's direct product decomposition.[26] As a result, (19) starts to generate equations of a new type. *First we consider the q_m exponentials of (19),* yielding for the bulk secular matrix

$$\mathbb{A}(\mathbf{k}_m)[\mathbf{u}_{mw}]=[\mathbf{0}], \quad (21)$$

where the quantities between the square brackets relate to the composite vectors, as described before. From (21) only nontrivial solutions can be obtained, if the bulk secular determinant becomes zero:

$$\|\mathbb{A}(\mathbf{k}_\parallel,q_m)\|=0. \quad (22)$$

The bulk secular determinant starts the normal-mode decomposition and double-cell method by generating the q_m. This is a tedious exercise, since q_m has to be found through a nonlinear, complex root-searching routine. The size of the bulk secular determinant-matrix for the case of a simple crystalline bulk can be reduced considerably by using the commensurability theorem proven by us.[25] After a root q_m has been found, one solves the eigenvector problem (21), yielding the normal-mode strengths $\mathbf{u}_{mw}$. *Knowing this, we consider the k_{pq} exponentials of Eq. (19).* Such consideration yields, in principle, infinite composite vector equations, but for optics, investigation of the κ_{00} exponential suffices. Since κ_{00} happens to equal k_z, the right-hand side of (19) will accidentally be involved, too. Hence,

$$-\alpha_0^{-1}\sum_{m=1}^{M}\nu_m\sum_{w=1}^{N_B}\left[\frac{e^{-i(\mathbf{k}\mathbf{r}_w^B+k_zd_S)}\overleftrightarrow{\mathbf{d}}_{00}}{1-\exp(i[q_m-k_z]d_B)}\right]\mathbf{u}_{mw}$$
$$-\alpha_0^{-1}\sum_{i=1}^{N_S}e^{-i\mathbf{k}\mathbf{r}_i}\overleftrightarrow{\mathbf{d}}_{00}\mathbf{p}_i=E_0\hat{\mathbf{e}}. \quad (23)$$

Index V has disappeared, since in (19) the exponential $\exp(i\mathbf{k}\mathbf{r}_v^B)$ can be divided out in the case of the κ_{00} exponential. Also, index V disappears in (23) and a single-vector equation is left. We emphasize again[21] that (23) has to be seen as the direct equivalent of the Ewald-Oseen extinction theorem, since it involves the incoming electromagnetic wave. The summation over the surface region has been explicitly neglected by Ewald, but typical surface optical effects stem from this summation.

The best way to understand the mechanism of the DC method is to start from a fictitious calculation, where the

free surface layer is considerably different from the bulk and the matching layer is missing. Using the unabridged normal-mode decomposition for the bulk region, many normal modes will be obtained, from which only those having a positive real part of the normal-mode vector q_m (semi-infinite system) will be relevant. The real part of the $\mathbf{q}_m$ remains confined to the interval $[-\pi/d_B, \pi/d_B]$, since $\mathbb{A}(\mathbf{k}_\parallel, q_m)$ is periodic with respect to the real part of q_m. Mostly, a q_m will be found near some κ_{pq}. Hence, apart from the two q_m being close to $\kappa_{00}=k_z$, all other q_m will be predominantly imaginary for optical frequencies. Only those two modes will survive a distance of about 10 interplanar distances, following the free surface layer. By incorporating these bulk layers into the surface layer as a matching layer, we will be left in the rest of the bulk with only two normal modes. The tremendous reduction in number of normal modes to only two that is thereby obtained explains the outstanding efficiency of the DC method. This means also that to the equations, which will control the surface layer (25), two equations have to be added to obtain the two normal-mode strengths ν_m of the bulk region. Since Eq. (23), however, adds three complex equations, the system of equations will become dependent. Exploiting the projection properties of $\mathbf{d}_{00}$ (Appendix B), the dependency can be removed by projection onto two independent vectors perpendicular to $\mathbf{k}$. Simply choosing the vectors $\hat{\mathbf{s}}$ and $\hat{\mathbf{p}}$ (generic $\hat{\mathbf{t}}$) for this projection, leaves us with the solvable system of equations

$$\frac{ik^2}{2\epsilon_0|\mathbf{s}_1\mathbf{x}\mathbf{s}_2||k_z|}\left[-\sum_{m=1}^{2}(e^{-ik_z d_S}\hat{\mathbf{t}}\cdot\mathbf{P}_m^B)\nu_m - \sum_{j=1}^{N_S} e^{-i\mathbf{k}\mathbf{r}_j}\hat{\mathbf{t}}^T\mathbf{p}_j\right]=E_0(\hat{\mathbf{t}}\hat{\mathbf{e}}) , \tag{24a}$$

$$\mathbf{P}_m^B=\mathbf{P}_m^B(\mathbf{k})=\frac{\sum_{w=1}^{N_B} e^{-i\mathbf{k}\mathbf{r}_w^B}\mathbf{u}_{mw}}{1-\exp(i[q_m-k_z]d_B)} . \tag{24b}$$

Two single complex equations remain. The projection used to arrive at (24) is the first step in matching the real-space approach of the surface layer and the normal-mode approach of the bulk. It remains only to derive the interaction equations for a *dipole located in the surface region*. Straightforward use of (10) yields

$$\mathbf{p}_i=\overleftrightarrow{\alpha}_i\left[E_0\hat{\mathbf{e}}e^{i\mathbf{k}\mathbf{r}_i}+\alpha_0^{-1}\sum_{j=1}^{N_S}\overleftrightarrow{\mathbf{f}}_{ij}\mathbf{p}_j + \alpha_0^{-1}\sum_{W=0}^{\infty}\sum_{w=1}^{N_B}\overleftrightarrow{\mathbf{f}}_{iWw}\mathbf{p}_{Ww}\right] . \tag{25}$$

Use (10b), (15), and (18) to reorganize (25) to

$$\overleftrightarrow{\alpha}_i^{-1}\mathbf{p}_i-\alpha_0^{-1}\sum_{j=1}^{N_S}\overleftrightarrow{\mathbf{f}}_{ij}\mathbf{p}_j-\alpha_0^{-1}\sum_{m=1}^{2}\mathbf{g}_i^m\nu_m=E_0\hat{\mathbf{e}}e^{i\mathbf{k}\mathbf{r}_i} , \tag{26a}$$

$$\underline{\mathbf{g}}_i^m=\sum_{w=1}^{N_B}\sum_{pq}^{\infty}\frac{e^{i[\mathbf{k}_{pq}(\mathbf{r}_i-\mathbf{r}_v^B)+\kappa_{pq}d_S]}}{1-\exp(i[q_m-\kappa_{pq}]d_B)}\overleftrightarrow{\underline{\mathbf{d}}}_{pq}\mathbf{u}_{mw} . \tag{26b}$$

Combining (24) and (26) yields the total DC interaction matrix

$$\begin{vmatrix}\mathbb{M}_{SS} & \mathbb{M}_{SB}\\ \mathbb{M}_{BS} & \mathbb{M}_{BB}\end{vmatrix}\begin{vmatrix}\mathbf{p}_i\\ \nu_m\end{vmatrix}=\begin{vmatrix}\mathbf{E}_i\\ \mathcal{E}_m\end{vmatrix} . \tag{27}$$

$\mathbb{M}_{SS}$ is a composite $(N_S\times N_S)$ matrix of transfer tensors and $\mathbb{M}_{BB}$ is a simple (2×2) complex matrix. The off-diagonal matrices have dimensions lining up with the two previous blocks. The inhomogeneous vector belonging to the normal-mode part $\mathcal{E}_m$ is, in practice, the s and the p component of the incoming light. The s-p factorization of the DC interaction equations will be proven in Sec. II D. The matrix elements of (27) can be obtained from Eqs. (24) and (26). The results of the DC method will be exact, within the assumptions of the discrete dipole theory.

C. Remote fields and reflection coefficients

The DC method yields directly semi-infinite reflection coefficients, since the basic main variables, $\mathbf{p}_i$ and ν_m, already relate to a semi-infinite system. Using (9), the remote electric field $\mathbf{E}_{\mathrm{REM}}$ at a point $\mathbf{r}$ in the vacuum half space follows from

$$\mathbf{E}_{\mathrm{REM}}(\mathbf{r})=\alpha_0^{-1}\left[\sum_{j=1}^{N_S}\overleftrightarrow{\mathbf{f}}_j(\mathbf{r})\mathbf{p}_j+\sum_{W=0}^{\infty}\sum_{w=1}^{N_B}\overleftrightarrow{\mathbf{f}}_{Ww}(\mathbf{r})\mathbf{p}_{Ww}\right] . \tag{28}$$

For the transfer tensors we need (15). Moreover, since only the 00 term in (15) involves a plane wave with real κ_{pq} (all other terms will be strongly evanescent) and we are only interested in remote fields, they all obey

$$\overleftrightarrow{\mathbf{f}}_j(\mathbf{r})=\overleftrightarrow{\underline{\mathbf{d}}}_{00}\exp(i\underline{\mathbf{k}}[\mathbf{r}-\mathbf{r}_j]) . \tag{29}$$

Using (14) and (16) yields the expression for the remote field

$$\mathbf{E}_{\mathrm{REM}}(\mathbf{r})=\frac{2\pi i a^3}{\alpha_0|\mathbf{s}_1\mathbf{x}\mathbf{s}_2||\mathbf{k}_z|}e^{i\mathbf{k}\mathbf{r}}[k^2\overleftrightarrow{\mathbf{1}}-\underline{\mathbf{k}}\underline{\mathbf{k}}^T]\mathbf{P}(\underline{\mathbf{k}}) , \tag{30a}$$

$$\mathbf{P}(\mathbf{k})=\left[\sum_{j=1}^{N_S}e^{-i\mathbf{k}\mathbf{r}_j}\mathbf{p}_j+\sum_{m=1}^{2}e^{-ik_z d_S}\mathbf{P}_m^B(\mathbf{k})\nu_m\right] . \tag{30b}$$

Projecting this result onto the reflected polarization direction $\hat{\mathbf{t}}=\hat{\mathbf{s}}$, $\hat{\mathbf{p}}$ and dividing the result by the (complex) electric-field strength $E_0\exp(i\underline{\mathbf{k}}\mathbf{r})$, yields the proper expression for the semi-infinite reflection coefficient r_t:

$$r_t=\frac{2\pi i a^3 k^2}{|\mathbf{s}_1\mathbf{x}\mathbf{s}_2||k_z|}\left[\frac{\hat{\mathbf{t}}\cdot\mathbf{P}(\underline{\mathbf{k}})}{\alpha_0 E_0}\right] . \tag{31}$$

The DC method is rather involved from the mathematical point of view, but lacks several nuisances, such as boundary conditions, that occur in continuum or hybrid approaches. SIOA is the difference in optical response for $\Omega=90°$ and $0°$.

1. The ellipsometric angles Ψ and Δ

For off-normal-incidence-reflection spectroscopy, mostly ellipsometric observation is preferred. Standard equations yield the ellipsometric angles Ψ and Δ, once the reflection coefficients are known:

$$r_s/r_p = \tan\Psi e^{i\Delta} . \tag{32}$$

In our convention, Δ will run from 0 to π if the angle of incidence θ is varied from 0 to $\pi/2$.

2. Comparison with the TS method

The key expression of the TS method[24] giving the semi-infinite reflection r, is

$$r = \frac{t_A r_B - \exp[iq_z(d_B - d_A)]t_B r_A}{t_A - \exp[iq_z(d_B - d_A)]t_B} . \tag{33}$$

r and t refer to reflection and transmission coefficients, respectively, of slabs A and B, having thicknesses d_A and d_B, and q_z the macroscopic Fresnel wave number in normal direction. Appendix C proves that (33) holds also for off-normal incidence.

D. Factorization

Interaction equations controlling the optical response from (110) surfaces of fcc crystals turn out to factorize, allowing for independent treatment of s- and p-type response. We will only discuss the $\Omega = 90°$ case ($k_x = 0$) as an example. For factorization, all matrix elements having a single x index should disappear. This we will investigate first for the secular matrix $\mathbb{A}$ (20) and the transfer tensors $\mathbf{f}_{ij}$ (10a) and (10b). The α tensors are diagonal throughout by assumption. The $\mathbf{c}$ tensors are also diagonal (no proof). The dyads in (20), (15), and (16) factorize if the xy, xz, yx, and zx components disappear and this holds if the summation over p turns out to be antisymmetric in p for given q. From Appendix A we know that

$$k^x_{-pq} = -k^x_{pq} , \quad \kappa_{pq} = \kappa_{-pq} . \tag{34a}$$

So it turns out that the xy, xz, yx, and yz components of the dyads $\mathbf{d}_{pq}$ are antisymmetric in p and their contributions to (20), (15), and (16) will disappear if the phase factors in the p summation are symmetric in p. This is the case since, for the phase factors of the x direction the following holds:

$$e^{ipg_1(x_i - x_j)} = \begin{cases} e^0 , & (x_i - x_j) = 0 , \\ e^{ip\pi} , & (x_i - x_j) = a/2 . \end{cases} \tag{34b}$$

In this way, it turns out that the secular matrix $\mathbb{A}$ and transfer tensors $\mathbf{f}_{ij}$ factorize into x and yz blocks for $\Omega = 90°$. As a result of the factorization of $\mathbb{A}$ the calculation of the normal modes takes place in two orthogonal subspaces coinciding with the plane of incidence (p space) and with the s direction (s space). Each subspace will yield its own $\mathbf{u}_m$, identified correspondingly as $\mathbf{u}_s$ and $\mathbf{u}_p$. The common meaning of the p label follows, taking into account the projection properties of the $\mathbf{d}_{00}$ (Appendix B). The factorization of the $\mathbf{f}_{ij}$ immediately certifies the factorization of the SS part of the DC interaction matrices. Since $\hat{\mathbf{x}}$ and $\hat{\mathbf{s}}$ are identical and both $\mathbf{u}_p$ and $\hat{\mathbf{p}}$ belong to the yz plane, factorization of the BS and BB parts, as given by (24), is obvious, too. Similar arguments as used before suffice to show the factorization of the SB part given by (27), as follows from investigation of (26). So for reflection from (110) surfaces of fcc crystals rigorous factorization takes place in the discrete model and $\mathbf{u}_s$ will always be at right angles with $\mathbf{k}$, $\underline{\mathbf{k}}$, $\mathbf{k}_m$ and $\mathbf{u}_p$.

III. NUMERICAL RESULTS

In this section we will treat some results obtained by means of the discrete dipole theory, as developed in the previous sections, where the emphasis will be on the microscopy and anisotropy of the angular-dependent reflection problem. For any quantity X dependent on Ω we will define the anisotropic difference ΔX as $X(\Omega = 90°) - X(\Omega = 0°)$. Unfortunately, the literature is not very consistent with respect to optical anisotropy terminology. A good overview about the issue can be found in two review articles.[29,30] We have made the following choices. The anisotropic reflectance difference (ARD) ΔR will always be defined as above with $X = R$, R being the reflectance r^*r. The important quantity is the relative anisotropic reflectance difference (RARD) defined as $\Delta R/R_0$, where R_0 will be the Fresnel reflectance value. This quantity comes closest to the reflectance anisotropy measured by the experimentalists. The differential reflectance will not be considered in this paper.[29] Finally, the anisotropic difference of the ellipsometric angles Ψ and Δ will be written as $\delta\Psi$ and $\delta\Delta$.

All cases to be studied as numerical results will obey the standard configuration, i.e., the systems will be made up from simple fcc (110)-oriented lattice planes. Polarizabilities have been found from dielectric constants by means of the Lorentz-Lorenz relation. The dielectric constants have been derived from the electronic structure, as obtained from density-functional pseudopotential calculations. Kramers-Kronig transforms have been used to yield the real from the imaginary part of the dielectric constant. For the bulk this approach is standard,[31,32] but for the surface the results from the electronic structure calculation follow as the auxiliary integral $I(\omega)$. Equation (16) of Ref. 24 has been used to convert $I(\omega)$ into surface dielectric constants, using $N_S = 3$ for the number of (free) surface planes. The dielectric constants for surface and bulk can be found for Si(110) in Ref. 32. The surface and bulk polarizabilities for GaP and GaAs(110) are similar to the ones used in Ref. 31, but in Ref. 31, arbitrary units have been used. Proper scaling can be used such that at $\hbar\omega = 4.0$ eV the imaginary part of α_{xx} becomes 0.022 714 for GaP and 0.021 403 for GaAs in units of α_0.

Further, two atoms will correspond to one dipole. This has been done for two reasons. First, the Lorentz-Lorenz equation does not allow one to assign polarizabilities to any of the constituents separately for the III-V compounds. Second, and this holds particularly for Si, this choice reduces the influence of the nondipolar interac-

tions, omission of which makes a one-atom-per-dipole assignment produce significantly worse results.[8]

A. Microscopic quantities and comparison of methods

The bulk value of the wave number can depend on the polarization[33] for cubic crystals only in continuum treatments going beyond the traditional approach. Recently, we have shown for the case of perpendicular incidence that the discrete dipole model results in anisotropic bulk optical response in a very direct way. The origin of this faint bulk anisotropy in cubic systems has to be sought in the disturbance of the static symmetry by the electromagnetic field. For this reason, we have shown in Fig. 2, for an angle of incidence of 75°, the difference between the absolute values of the normal-mode wave numbers q_m and the Fresnel wave number q_0 (results in units of $1/a$), for bulk Si. The two kinds of wave numbers are almost identical, differing less than 1% from the global value. Further, Fig. 2 shows on the left-hand side the differences for s- and p-polarized light if $\Omega=0°$ and on the right-hand side it shows the corresponding differences for $\Omega=90°$. At first glance it looks as if s and p polarizations have reversed roles going from left to right in Fig. 2. Careful study of the numerical data reveals that the resemblance is not perfect. For $\Omega=0°$ and s polarization the system becomes triggered along the y direction, but for $\Omega=90°$ and p polarization the system becomes triggered along the y and z directions. Nevertheless, roughly similar anisotropic differences are obtained, although z components are expected to decrease anisotropy. This is a remarkable conclusion since, at a 75° angle of incidence, the z component of the electric field exceeds the y component about four times.

An essential part of the microscopy is the behavior of the normal modes. Section II D concerning factorization yielded the orientation in space of $\mathbf{u}_s$. How $\mathbf{u}_p$ is exactly oriented in the p subspace to which it was found to be confined requires additional study. In macroscopic treatments, it has to be concluded from the divergence of the macroscopic field that this field and the refracted wave vector have to be at right angles, since the macroscopic charge density equals zero in dielectric systems. However the $\mathbf{p}$'s or $\mathbf{u}_m$'s are not simple substitutes for the macroscopic polarization field $\mathbf{P}$, causing a fundamental difference between the discrete and continuum approaches. To study the behavior of the $\mathbf{u}_p$ we have investigated for a photon energy of 3.0 eV transparent and absorbing model substrates. The substrates have polarizabilities obtained by means of Lorentz-Lorenz from an isotropic dielectric constant of 10.0 for transparent and from an isotropic dielectric constant of $25.0+i5.0$ for absorbing substrates. We start with a calculation of the two dot products $\hat{\mathbf{u}}_p\cdot\hat{\mathbf{k}}$ and $\hat{\mathbf{u}}_p\cdot\hat{\mathbf{k}}_m$ as a function of angle of incidence θ_i for the transparent model substrate. For the transparent substrate these dot products are real and the angle between $\hat{\mathbf{u}}$ and $\hat{\mathbf{k}}$, $\hat{\mathbf{k}}_m$ can be found from these dot products in a meaningful way. The angles are shown in Table I, where we subtracted also 90° in order to highlight orthogonality. It is obvious that $\hat{\mathbf{u}}_p$ comes only to orthogonality with $\hat{\mathbf{k}}_m$ for all angles of incidence. On the other hand, this orthogonality is not perfect. The values are at least 11 orders of magnitude above the digital noise level. So the proper statement has to be that within the framework of a discrete dipole approach, the $\hat{\mathbf{u}}_p$ are almost at right angles to the refracted $\hat{\mathbf{k}}_m$, obviously in good agreement with what one expects from the classical approaches.

We also want to find out what happens with this statement when the material becomes absorbing. So we have calculated again the dot product $\hat{\mathbf{u}}\cdot\hat{\mathbf{k}}_m$ as a function of angle of incidence for the absorbing model substrate. The dot product is shown in Table II as it is, since a complex angle will not add much to our understanding. In absolute value, the absorbing dot product $\hat{\mathbf{u}}_p\cdot\hat{\mathbf{k}}_m$ is about

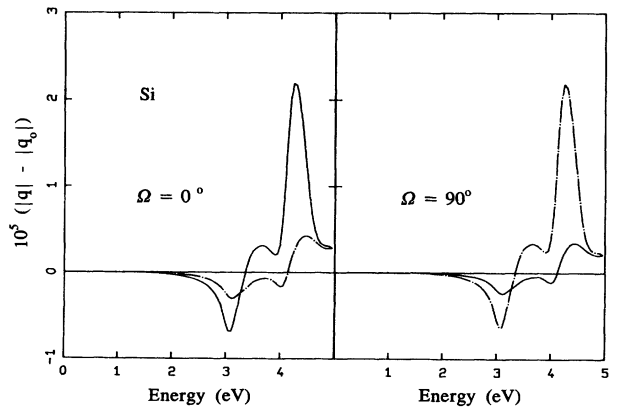

FIG. 2. Difference between discrete dipole and Fresnel wave numbers as a function of energy for Si in units of $1/a$. $\theta_i=75°$; ——, s polarization; —·—·—·, p polarization; left-hand side, $\Omega=0°$, right-hand side, $\Omega=90°$.

TABLE I. Orthogonality of $\hat{\mathbf{u}}_p$ with respect to $\hat{\mathbf{k}}$ or $\hat{\mathbf{k}}_m$ for a transparent substrate with $\epsilon=10.0$ and $\hbar\omega=3.0$ eV for various θ_i.

No.	θ_i	$<(\hat{\mathbf{u}}\cdot\hat{\mathbf{k}})-90$	$<(\hat{\mathbf{u}}\cdot\hat{\mathbf{k}}_m)-90$
	$\Omega=0°$		
1	0.000°	0.000 000 00°	$(-3.885\,780\,59\times10^{-16})°$
2	30.000°	−20.902 449 84°	$(-8.738\,321\,07\times10^{-5})°$
3	60.000°	−44.105 540 56°	$(-1.319\,007\,98\times10^{-4})°$
4	85.000°	−66.637 321 09°	$(-1.411\,843\,52\times10^{-4})°$
	$\Omega=90°$		
1	0.000°	0.000 000 00°	$(-3.885\,780\,59\times10^{-16})°$
2	30.000°	−20.902 143 88°	$(4.254\,585\,26\times10^{-5})°$
3	60.000°	−44.105 154 39°	$(6.013\,638\,97\times10^{-5})°$
4	85.000°	−66.636 953 40°	$(6.185\,678\,55\times10^{-5})°$
$\hbar\omega=3.0$ eV		$\epsilon=10.0+i0.0$	

TABLE II. Dot product $\hat{\mathbf{u}}_p \cdot \mathbf{k}_m$ for an absorbing substrate, $\epsilon = 25.0 + i5.0$ and $\hbar\omega = 3.0$ eV for various θ_i.

No.	θ_i	$\hat{\mathbf{u}} \cdot \hat{\mathbf{k}}_m$
	$\Omega = 0°$	
1	0.00°	$-1.001\,07 \times 10^{-17} + i - 1.220\,78 \times 10^{-18}$
2	30.00°	$2.646\,83 \times 10^{-6} + i5.647\,96 \times 10^{-7}$
3	60.00°	$4.350\,36 \times 10^{-6} + i9.753\,34 \times 10^{-7}$
4	85.00°	$4.875\,09 \times 10^{-6} + i1.120\,04 \times 10^{-6}$
	$\Omega = 90°$	
1	0.00°	$-1.001\,08 \times 10^{-17} + i - 1.220\,10 \times 10^{-18}$
2	30.00°	$-1.310\,09 \times 10^{-6} + i - 2.822\,22 \times 10^{-7}$
3	60.00°	$-2.105\,91 \times 10^{-6} + i - 4.868\,29 \times 10^{-7}$
4	85.00°	$-2.332\,51 \times 10^{-6} + i - 5.586\,83 \times 10^{-7}$
$\hbar\omega = 3.0$ eV		$\epsilon = 25.0 + i5.0$

twice as large, as compared to the transparent case. So even as complex quantities the two vectors $\hat{\mathbf{u}}_p$ and $\hat{\mathbf{k}}_m$ are almost at right angles. In the discrete model, it is a far from straightforward exercise to show this by explicit calculation. The differences increase rather precisely with k^2, in good agreement with our earlier findings. The absence of perfect orthogonality of refracted wave vector and polarization has to be ascribed in the discrete approach to bulk local-field effects. The same phenomenon is also known from continuum treatments.

To finish the treatment of the behavior of the normal modes, the bulk Brewster minimum will be studied. In view of expression (31) for the reflection, the reflection can only become zero if the dot product $\hat{\mathbf{t}} \cdot \mathbf{P}(\underline{\mathbf{k}})$ vanishes. The proper Brewster angle will be obtained if $\hat{\mathbf{t}}$ and $\mathbf{P}(\underline{\mathbf{k}})$ are perpendicular. Disregarding the dipoles in the surface layer, we will verify this for the contribution of the bulk normal modes to $\mathbf{P}(\underline{\mathbf{k}})$. In Table III, we have collected some results concerning the relevant dot product $\hat{\mathbf{u}}_p \cdot \hat{\underline{\mathbf{p}}}$, converted into an angle for the transparent model substrate. We see that the angle where the two vectors $\hat{\underline{\mathbf{p}}}$ and $\hat{\mathbf{u}}_p$ are exactly at right angles coincides with the classical Brewster angle, 72.45° in this case. For the two main azimuthal orientations, there is a small anisotropy in the Brester angle of $(3.4 \times 10^{-4})°$. If we confine ourselves to bulk cases only and consider simple continuum treatments to be sufficient, it does not make any difference whether for the Brewster angle criterion, orthogonality of $\hat{\mathbf{u}}_p$ and $\hat{\underline{\mathbf{p}}}$ or orthogonality of $\hat{\underline{\mathbf{k}}}$ and $\hat{\mathbf{k}}_m$ is considered. In view of the results of Tables I and II, the two criteria, however, cannot be identical. This conclusion follows directly from the discrete approach, but the remark as such is also known from more elaborate continuum treatments. Since for transparent media the dot product happens to be a simple real number, it suffices to use continuity to prove the occurrence of a zero. For absorbing media we see that the zero occurs only in the real part of the dot product, whereas the imaginary part keeps a nonzero value. As a result, only a minimum can be found in the reflection. In principle the zero in the real part can be used to define and/or locate the Brewster angle for absorbing substrates. Returning

TABLE III. Orthogonality of $\hat{\mathbf{u}}_p$ and $\hat{\underline{\mathbf{p}}}$ for a transparent substrate ($\epsilon = 10.0$) and the dot product $\hat{\mathbf{u}}_p \cdot \hat{\underline{\mathbf{p}}}$ for absorbing substrate ($\epsilon = 25.0 + i5.0$) at $\hbar\omega = 3.0$ eV, both for various θ_i.

No.	θ_i	$<(\hat{\mathbf{u}} \cdot \hat{\underline{\mathbf{p}}}) - 90$	$\hat{\mathbf{u}} \cdot \hat{\underline{\mathbf{p}}}$
	$\Omega = 0°$		
1	0.000	−90.000 00°	$1.000\,000 + i - 2.304\,824 \times 10^{-36}$
2	30.000	−50.902 45°	$8.125\,001 \times 10^{-1} + i5.714\,473 \times 10^{-3}$
3	60.000	−14.105 54°	$3.448\,126 \times 10^{-1} + i1.609\,349 \times 10^{-2}$
4	72.250	$(-2.215\,143 \times 10^{-1})°$	
5	72.500	$(5.359\,128 \times 10^{-2})°$	
6	78.750		$1.850\,776 \times 10^{-3} + i1.949\,825 \times 10^{-2}$
7	79.000		$-2.680\,720 \times 10^{-3} + i1.951\,559 \times 10^{-2}$
8	85.000	13.362 68°	$-1.100\,815 \times 10^{-1} + i1.969\,606 \times 10^{-2}$
	$\Omega = 90°$		
1	0.000	−90.000 000°	$1.000\,000 + i - 1.411\,876 \times 10^{-52}$
2	30.000	−50.902 14°	$8.124\,890 \times 10^{-1} + i5.711\,396 \times 10^{-3}$
3	60.000	−14.105 15°	$3.447\,854 \times 10^{-1} + i1.608\,504 \times 10^{-2}$
4	72.250	$(-2.211\,373 \times 10^{-1})°$	
5	72.500	$(5.396\,806 \times 10^{-2})°$	
6	78.750		$1.819\,744 \times 10^{-3} + i1.948\,804 \times 10^{-2}$
7	79.000		$-2.711\,764 \times 10^{-3} + i1.950\,537 \times 10^{-2}$
8	85.000	13.363 05°	$-1.101\,125 \times 10^{-1} + i1.968\,571 \times 10^{-2}$
$\hbar\omega = 3.0$ eV		$\epsilon = 10.0$	$\epsilon = 25.0 + i5.0$

to the transparent cases, we add that the vanishing reflection for the bulk at the Brewster angle relates to the vanishing emission due to vanishing $\hat{\mathbf{u}}\cdot\hat{\mathbf{p}}$ for each bulk layer separately. Adding the surface layers to $\mathbf{P}(\underline{\mathbf{k}})$ changes our treatment of the Brewster angle, but the global picture remains the same. Even monolayers display a clear Brewster minimum, for instance. Explaining the Brewster angle in the discrete approach primarily involves an analysis of the emission process after the interaction equations have been solved. Only the precise location of the minimum itself is determined by the interaction equations and escapes as such from a simple straightforward analysis.

The direct accessibility of microscopic quantities such as individual dipole strengths or absorbances is one of the attractive aspects of the discrete dipole approach. In Fig. 3 we show the absolute values of the individual dipole strengths of the 32 outermost layers of a semi-infinite Si sample, all obtained for an energy of 3.0 eV and an angle of incidence of 75°. The polarizabilities used are listed in Table IV. The dipole strengths are given in units of $p_0=\alpha_0 E_0$. In their global appearance, there is hardly any difference between the two orientations of the anisotropic azimuth. Only more careful observation reveals that in those cases where polarization becomes induced in the y direction, chains perpendicular to the surface (corresponding to $\Omega=90°$, p polarization or $\Omega=0°$, s polarization) exhibit the stronger deviations in the surface area with respect to bulk. Those deviations are characteristic for the outermost layers, called the wiggling zone because the deviations turn into wiggles at higher frequencies. It is noteworthy that just as the reflection goes through the Brewster minimum due to the disappearance of the dot product $\hat{\mathbf{t}}\cdot\mathbf{P}(\underline{\mathbf{k}})$, for p polarization the modulus of the individual dipoles $\mathbf{p}_i$ increases by over a factor of 2, as compared to the s-type equivalents. Most of the unexpected p-type behavior near the Brewster angle of SIOA that cannot be reduced to differences between the values of the components of α stems from this fact.

Next, we have plotted in Fig. 4 the anisotropic dipole strength difference $\Delta|\mathbf{p}(i)|$ for the two polarizations. Clearly, the variations near the surface of this quantity are largest for the p component. Figure 4 shows the differences in length of the dipole strength vectors, not in orientation. Since the Brewster angle for reflection shows an anisotropy considerably larger than the angular anisotropy of the $\mathbf{u}_p$, as discussed before, it has to be concluded that the p-type dipole strengths for the two anisotropic azimuths have a slightly different orientation in the p plane, especially as concerns the near-surface layers. So near the surface, both orientation and length of the individual dipole strengths show anisotropic variations for p polarization. For s polarization only length anisotropy occurs.

The absorbance issue is of fundamental importance.

TABLE IV. Bulk and surface polarizabilities for Si (110) at $\hbar\omega=3.0$ eV (in units of α_0).

α_B	$0.149\,721+i3.508\,82\times10^{-3}$
$\alpha_{S,x}$	$0.149\,231+i8.862\,95\times10^{-3}$
$\alpha_{S,y}$	$0.139\,966+i9.234\,19\times10^{-3}$
$\alpha_{S,z}$	$0.145\,399+i9.276\,44\times10^{-3}$
	$\hbar\omega=3.0$ eV

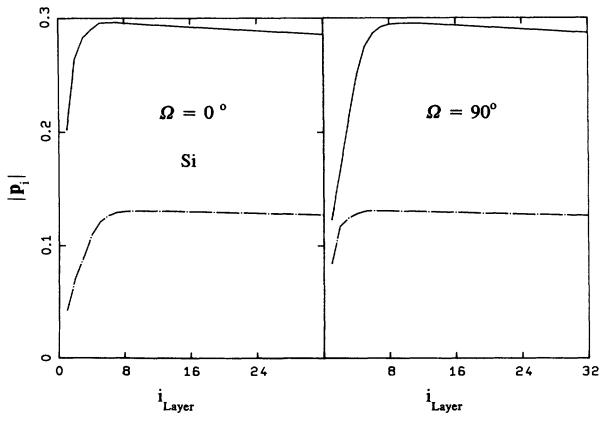

FIG. 3. Modulus of dipole strength $|\mathbf{p}_i|$ as a function of layer index i in units of $p_0=\alpha_0 E_0$, Si, $\hbar\omega=3.0$ eV, $\theta_i=75°$; —·—·—·, s polarization; ——, p polarization; left-hand side, $\Omega=0°$, right-hand side, $\Omega=90°$.

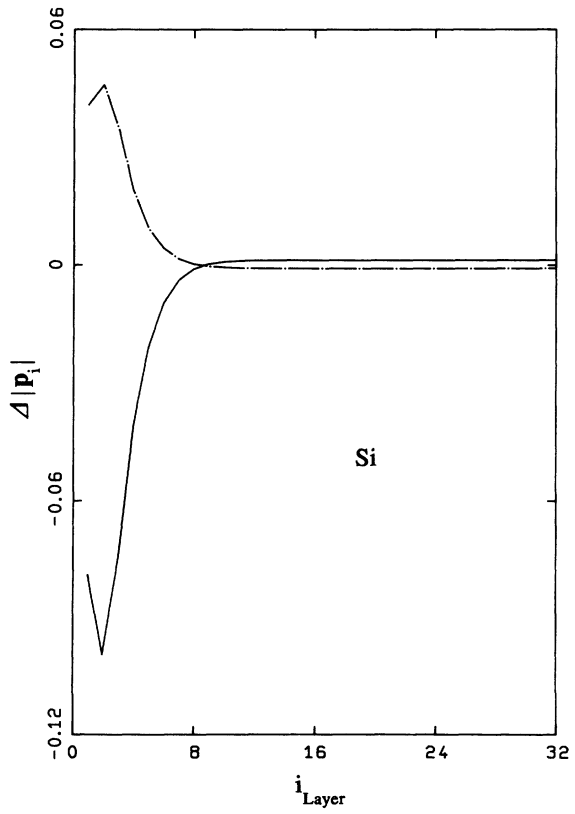

FIG. 4. Anisotropic difference dipole strength $\Delta|\mathbf{p}_i|=|\mathbf{p}_i(90°)|-|\mathbf{p}_i(0°)|$; —·—·—·, s polarization; ——, p polarization; otherwise as Fig. 3.

Most quantum-mechanical derivations of the dielectric constant rely upon absorption, mostly under the assumption that it depends weakly on place. Conservation of energy is usually for optics expressed as

$$A+R+T=1\ , \tag{35}$$

where R has been given before, $T=t^*t$ is the transmittance, and A the absorbance, usually found from (35). This absorbance A is a dimensionless quantity indicating which fraction of the incoming energy flux becomes absorbed in a slab or semi-infinite medium. For an individual layer, the local absorbance A_i is defined as

$$A=\sum_i A_i\ , \tag{36a}$$

$$A_i=-\frac{k^2}{\beta k_z \epsilon_0 a^2 |\mathbf{E}_0|^2}\mathrm{Im}(\mathbf{p}_i^{*T}\overleftrightarrow{\alpha}_i^{-1}\mathbf{p}_i)\ , \tag{36b}$$

and according to (36a) the total absorbance A can be calculated microscopically. The absorbances found from (35) and (36) turn out to be the same only up to the last digit, if the calculation incorporates the electromagnetic self-interaction of the dipole, as obtained by Lorentz.[34] We have systematically included the self-interaction in all our calculations (if included into the intraplanar transfer tensor it becomes canceled by an identical term). Absorbance builds a very critical test for the quality of discrete-dipole calculations. From slab calculations we know, e.g., that conservation of energy as stated by (35) is lost if the internal dipole fields are switched off. We show the local absorbances A_i in Fig. 5 for the same case shown in Fig. 3 (polarizabilities again from Table IV). The local absorbance differs in behavior strongly from the dipole strength. The most striking feature in Fig. 5 is the abrupt kink exactly after three dipole layers. This, however, is by no means surprising, since we have used explicitly in our calculations a simple rectangular profile with a width of three dipole layers. Since we know from Fig. 3 that the dipole strength behaves smoothly as a function of layer index, it is clear from (36b) that a rectangular profile for α is likely to yield a kink after three layers. So the real surprise is the smoothness of the dipole strength. Now in the x direction the striking phenomena occur. For $\Omega=0°$, p type and $\Omega=90°$, s type the local absorbance in the surface region exceeds by a factor of 2 the absorbance in the nearby bulk. It is obvious that such deviations can no longer be treated as small corrections in that area, but the results seem to be in disagreement with those shown in Fig. 3. This unexpected behavior is explained by the behavior of the polarizability. It is easy to see from (36b) that for a diagonal α the absorbance becomes determined by the imaginary part of α. For the x direction the imaginary part of the surface polarizability is almost twice as large as the corresponding bulk one (9.718 vs 4.717 in units of α_0). For the y direction this difference is small (5.099 vs 4.717). In connection with the smooth behavior of $|\mathbf{p}_i|$ the results of Fig. 5 are clear. In Fig. 6 we show the corresponding differences. Again, the p-type differences are by far the largest. Surprisingly, however, the differences no longer display the kink.

In order to test the reliability of the DC method for off-perpendicular cases, a comparison has been made with the TS method. Having studied many different cases, we found that the differences between the two methods is typically of the order of 10^{-5} as far as RARD results are concerned. These deviations are all due to

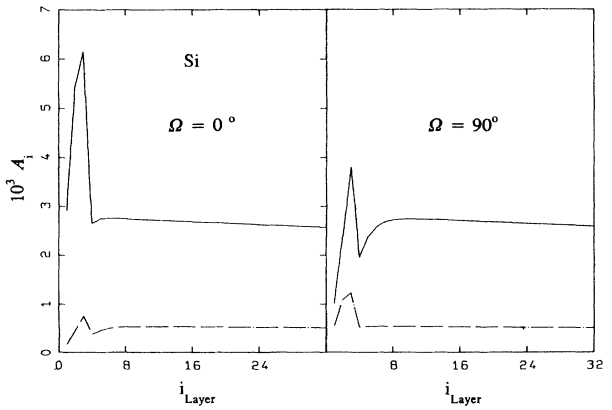

FIG. 5. Local absorbance A_i as a function of layer index i, Si, $\hbar\omega=3.0$ eV; $\theta_i=75°$; —·—·—·, s polarization; ——, p polarization; left-hand side, $\Omega=0°$; right-hand side, $\Omega=90°$.

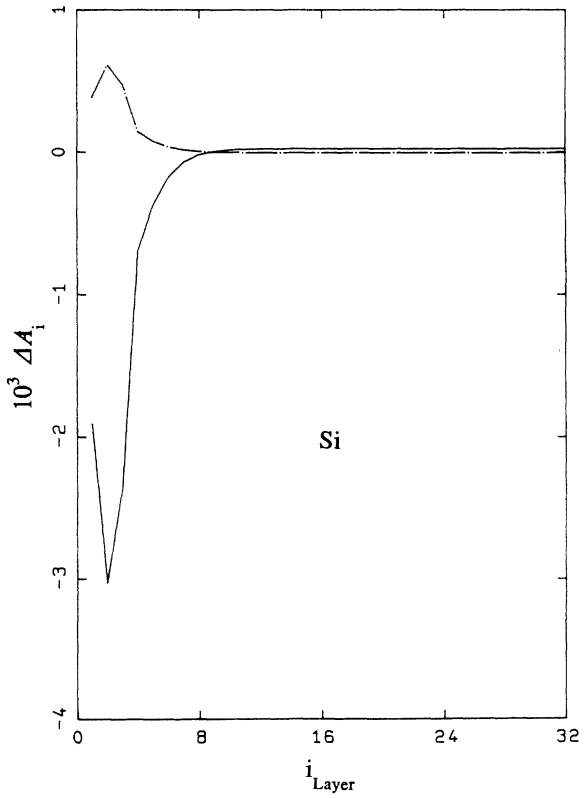

FIG. 6. Anisotropic difference local absorbance $\Delta A_i=A_i(90°)-A_i(0°)$; —·—·—·, s polarization; ——, p polarization; otherwise as Fig. 5.

small and insignificant imperfections in the implementation of the TS method. The DC method yields exact results within the basic assumptions of the discrete approach.

B. Macroscopic numerical results

Using the standard configuration mentioned at the beginning of Sec. III, we have calculated the angular-dependent anisotropic behavior as a function of frequency and angle of incidence for the elementary semiconductor Si and the two III-V compounds GaP and GaAs. Three angles of incidence have been used, i.e., 60°, 70°, and 80°, where the first always will correspond in the figures to the solid, the second to the dot-dashed, and the third to the dot-dot-dashed lines. For all those cases we will investigate the RARD for s and p polarization and the anisotropic difference in the ellipsometric angles Ψ and Δ.

Figure 7 shows for Si the s-type RARD for the three angles mentioned before. The overall shape of the spectra is identical to, but significantly smaller than, the perpendicular incidence results[24] obtained before. This further supports our previous remark[23] that not much is going to be accomplished measuring at off-normal angles of incidence. For a fixed frequency the angular-dependent behavior of the ARD has already been given in I. Although Fig. 7 displays only three angles of incidence, the conclusion is that the angular dependency of the s-type RARD does not depend much on energy. Figure 8 shows the p-type RARD as a function of energy for the same three angles. Different angles of incidence have stronger impact upon p-polarized anisotropy and affect particularly the p-type energy dependence. Most apparent is the reversal in sign passing from a 70° angle of incidence to 80°, due to the crossing of the Brewster angle. This reversal of sign is most clearly observed for the lower energies whereas, near 5 eV, this phenomenon tends to disappear. It is particularly noteworthy that the 60° results are lower in absolute value than the 70° results. This seems to violate the angular dependence found in I, but in this paper the experimentally preferred RARD is treated. The behavior of R_0 explains the deviations. The most striking feature in Fig. 8 is made up by the strong peak at 3.0 eV for an 80° angle of incidence. As argued already in I, semiconductors at low energies have almost dielectric behavior and the corresponding critical behavior near Brewster's angle. The anisotropic differences themselves are not affected by the phenomenon of the Brewster angle, it appears from the discrete dipole calculations. The ellipsometric SIOA data are shown for Si in Figs. 9 and 10. Figure 9 shows the behavior of $\delta\Psi$. In general, the results resemble those obtained for the p-type RARD as shown in Fig. 8, but with reversed sign, because the p

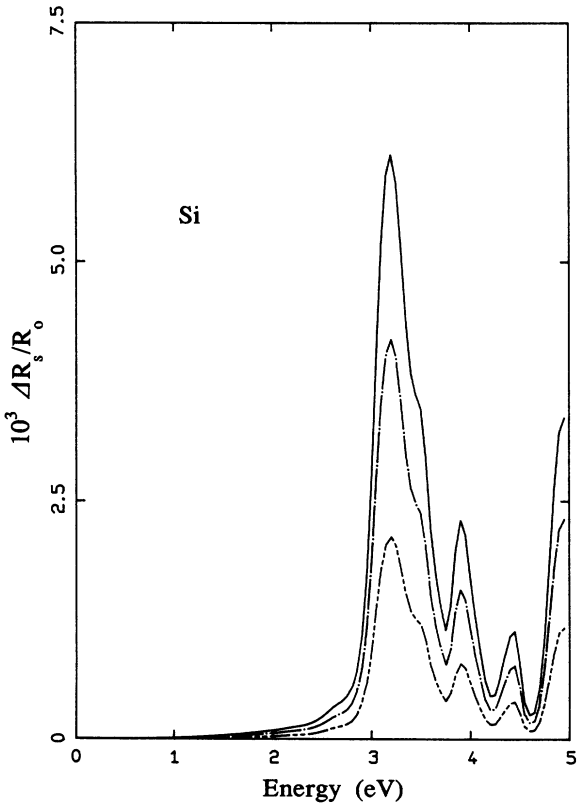

FIG. 7. Relative anisotropic reflectance difference $\Delta R_s/R_0$ as a function of energy, Si; s polarization; ——, $\theta_i=60°$; —·—·—·, $\theta_i=70°$; –··–··–, $\theta_i=80°$.

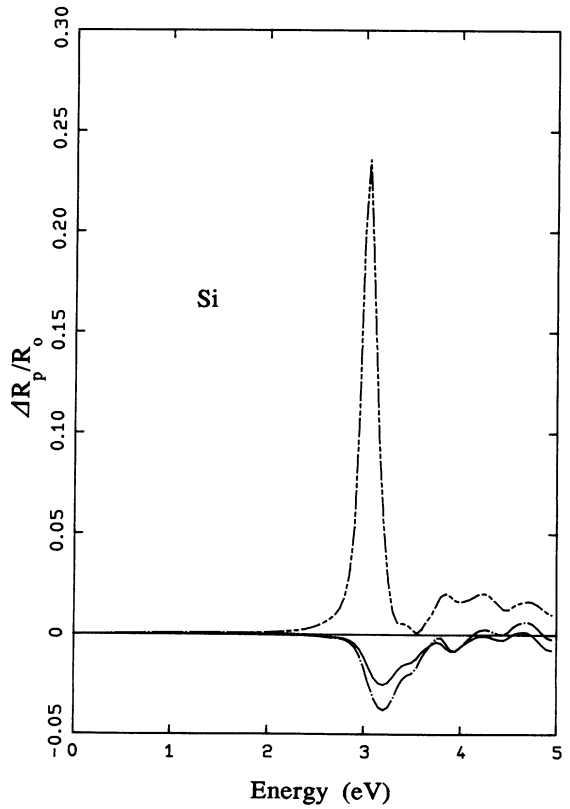

FIG. 8. Relative anisotropic reflectance difference $\Delta R_p/R_0$ as a function of energy, Si, p polarization; ——, $\theta_i=60°$; —·—·—·, $\theta_i=70°$; –··–··–, $\theta_i=80°$.

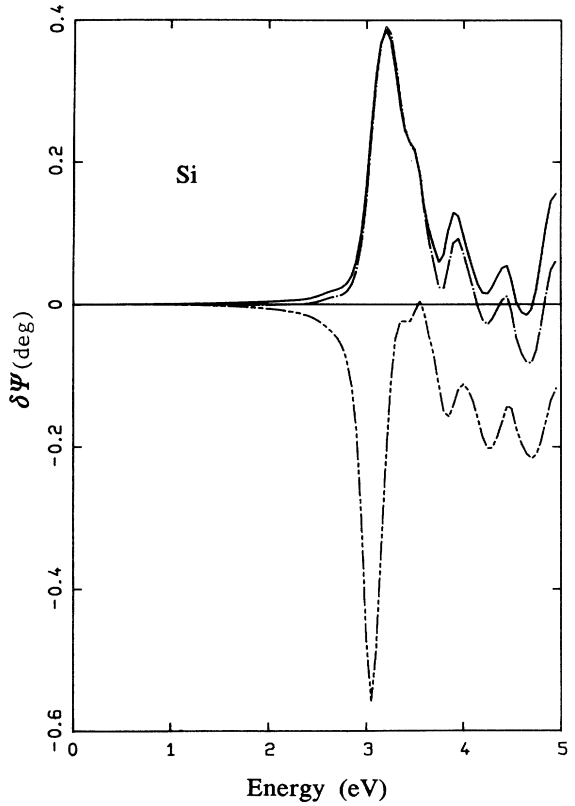

FIG. 9. Anisotropic ellipsometric difference angle $\delta\Psi$ as a function of energy, Si; ——, $\theta_i = 60°$; —·—·—·, $\theta_i = 70°$; —··—··—, $\theta_i = 80°$.

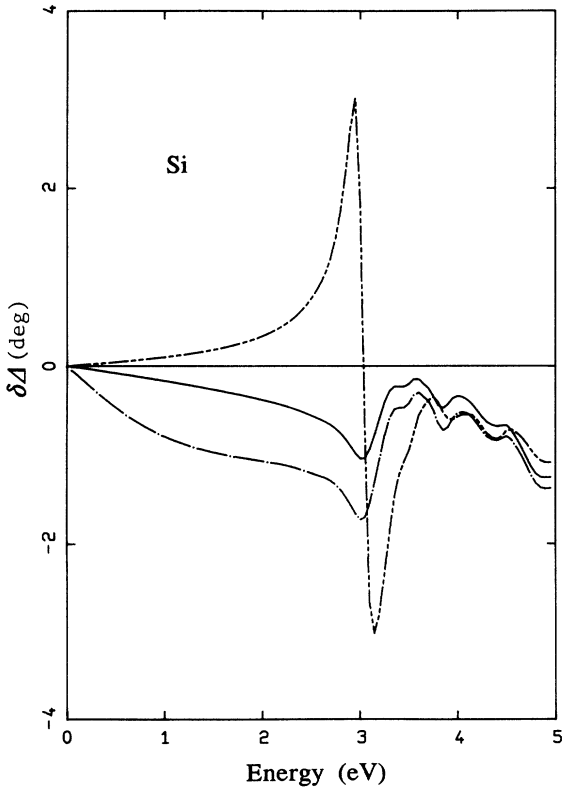

FIG. 10. Anisotropic ellipsometric difference angle $\delta\Delta$ as a function of energy, Si; ——, $\theta_i = 60°$; —·—·—·, $\theta_i = 70°$; —··—··—, $\theta_i = 80°$.

component enters the expression for Ψ through the denominator (32). The Ψ differences are a few tenths of a degree and should be easily measurable, if the angle of incidence repeatability were not a problem.[23] This remark applies even more to $\delta\Delta$ as shown in Fig. 10, being almost one order of magnitude larger than the corresponding $\delta\Psi$ data. The $\delta\Delta$ results do not resemble any of the results shown before, the main reason being the nonzero response for energies below the optical energy gap of Si. The measurement procedures used until now for the investigation of SIOA are only able to detect a signal if the system under investigation becomes absorbing. Measurement of the ellipsometric $\delta\Delta$ overcomes this problem. Recently, however, Wormeester *et al.*[35] have shown that also for perpendicular incidence, ellipsometric detection of SIOA can be used advantageously in experiment. The phase difference disappears for energies approaching zero. Since the angle Δ can be associated with the optical pathlength, expressed in wavelengths, it is easy to understand why this happens. The anisotropy introduces a rather constant difference in optical pathlength, whereas the wavelength goes to infinity for $\hbar\omega$ going to zero.

Figures 11 and 12 show the angular-dependent SIOA for GaP(110). In general, the results obey the behavior discussed already for Si. GaP is an indirect-gap III-V semiconductor, but with less difference between its direct and indirect gap than Si. This semiconductor is particu-

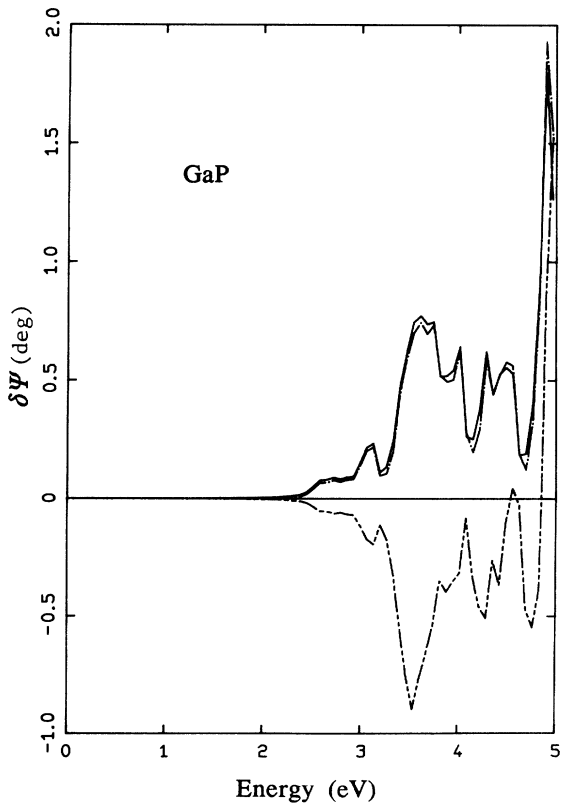

FIG. 11. Anisotropic ellipsometric difference angle $\delta\Psi$ as a function of energy, GaP; ——, $\theta_i = 60°$; —·—·—·, $\theta_i = 70°$; —··—··—, $\theta_i = 80°$.

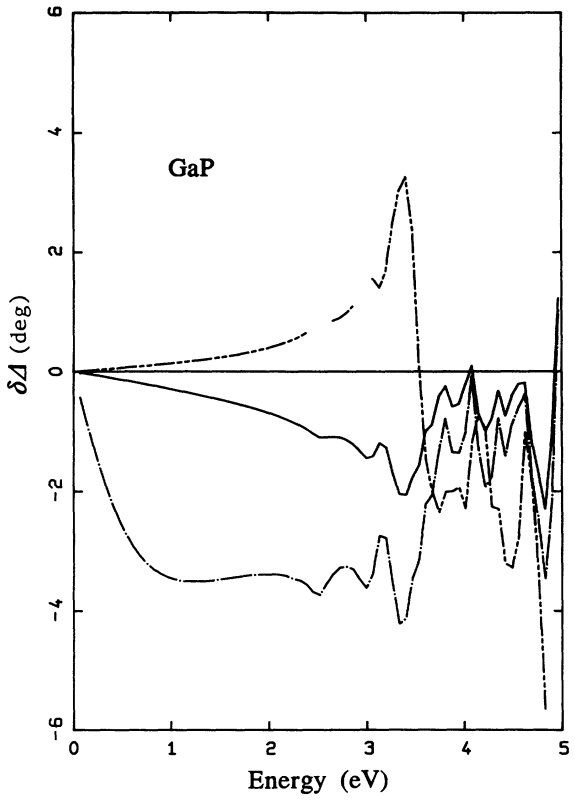

FIG. 12. Anisotropic ellipsometric difference angle $\delta\Delta$ as a function of energy, GaP; ——, $\theta_i = 60°$; —·—·—·, $\theta_i = 70°$; —··—··—, $\theta_i = 80°$.

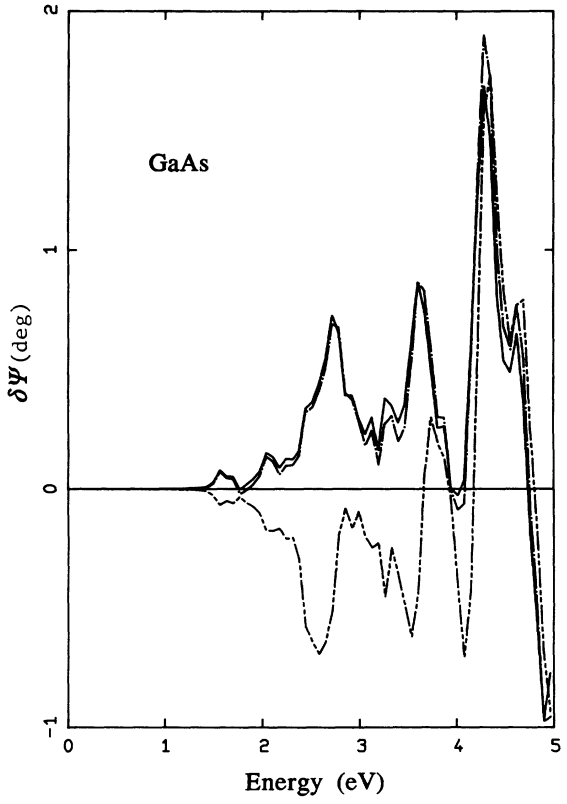

FIG. 13. Anisotropic ellipsometric difference angle $\delta\Psi$ as a function of energy, GaAs; ——, $\theta_i = 60°$; —·—·—·, $\theta_i = 70°$; —··—··—, $\theta_i = 80°$.

larly known for having surface-state transitions, being within the energy gap. The beginning of the transitions at 2.5 eV have been associated with $A5$-$C3$ surface states or resonances.[31] If we consider the absolute values of the p-type results, it can be seen that they are not as far apart as for Si. Again, Brewster's angle has to be located somewhere between 70° and 80° for all energies investigated. As for Si, the ellipsometric difference $\delta\Psi$ (Fig. 11) shows a particularly weak dependence from the angle of incidence, apart from the change in sign. The 60° and 70° results in particular are almost identical. As for the $\delta\Delta$ results shown in Fig. 12, again the subband-gap anisotropies are interesting, especially for a 70° angle of incidence. GaP displays there a phase anisotropy three times stronger than Si over almost the entire subband-gap energy range.

The last results concern the III-V semiconductor GaAs. The characteristic features of the SIOA response of GaAs(110) are the two peaks at 2.7 and 3.6 eV.[31] Apart from the $\delta\Delta$ results, this characteristic double-peak structure dominates all types of angular-dependent SIOA obtained from GaAs. The anisotropy in the two ellipsometric angles $\delta\Psi$ (Fig. 13) and $\delta\Delta$ (Fig. 14) follows the previous patterns, $\delta\Psi$ being almost invariant with respect to the angle of incidence, and $\delta\Delta$ having strong subband-gap values. The latter, however, are less strong than for GaP.

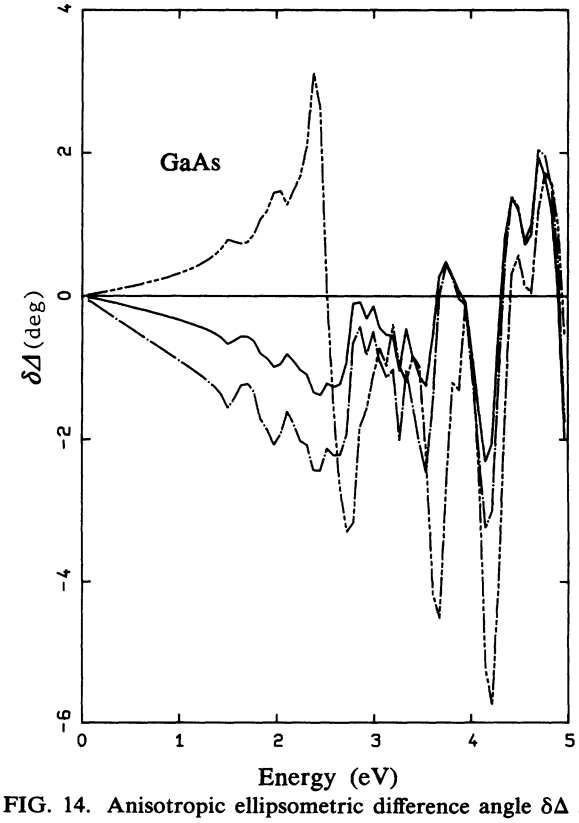

FIG. 14. Anisotropic ellipsometric difference angle $\delta\Delta$ as a function of energy, GaAs; ——, $\theta_i = 60°$; —·—·—·, $\theta_i = 70°$; —··—··—, $\theta_i = 80°$.

IV. CONCLUSIONS

It has been shown that the angular dependence of SIOA can be well described by means of the discrete dipole model using the DC method. The results obtained by the DC method are exact within the assumptions of the discrete dipole approach and confirmed by the TS method. Contrary to the *s*-type normal-mode eigenvector $\mathbf{u}_s$, the *p*-type eigenvector $\mathbf{u}_p$ is not exactly at right angles to the refracted wave vector $\mathbf{k}_m$. It has been found that, in general, the *p*-type response yields the more interesting results. The discrete model provides direct access to the microscopy of the semi-infinite problem, provided the DC method is used. Dipole strengths for *p*-polarized light turn out to be more than twice as strong near Brewster's angle than the *s*-type dipole strength. The Brewster minimum, itself, is caused by the projection occurring in the discrete dipole expression for reflection. Also, the anisotropy in dipole strength and reflection is larger for *p*-polarized than for *s*-polarized light. Absorption, local fields, and retardation are directly incorporated in the discrete approach to the surface reflection problem. Problems with boundary conditions or the necessity to distinguish explicitly between longitudinal and transversal modes, as known from continuum models, do not exist in discrete models. The spectroscopic anisotropic response has been calculated in detail for the (110) surfaces of the three important semiconductors Si,GaP, and GaAs. In general, the theoretical results favor measurements of SIOA at perpendicular incidence, as is usually the case now. Only near Brewster's angle for almost transparent substrates an increased sensitivity for SIOA can be found using *p*-polarized light. The additional experimental difficulties that have to be expected when using this advantage probably render the option only as a potential one.

ACKNOWLEDGMENT

We would like to thank Professor R. Del Sole from the Rome II University, for letting us use his quantum-mechanical calculations of the surface optical properties of the semiconductors treated in this paper.

APPENDIX A: THREEFOLD INTEGRAL TRANSFORM

Transfer tensors are obtained from scalar planar sums. The expression for the scalar planar sums[20] can, for this appendix, be written as (without prime)

$$S_j(\mathbf{r},\mathbf{k})=\sum_{mn}\exp(i\mathbf{k}\cdot\mathbf{s}_{mn})\exp(ik|\mathbf{r}-\mathbf{r}_{j,mn}|)/|\mathbf{r}-\mathbf{r}_{j,mn}| \ . \tag{A1}$$

Efficient evaluation of scalar planar sums $S_j(\mathbf{r},\mathbf{k})$ for points outside the plane itself is indispensible in advanced dipole theory. Ewald's threefold integral transform satisfies those needs. The original Ewald derivation,[36] however, is not general and is far from transparent, due to the old notation. An improved general derivation has been given by Litzman.[26] This appendix treats an equally general derivation, elucidating the role of the surface Brillouin zone. Suppose a function $f(\mathbf{r})$ being defined on $\mathbb{R}^3$, has two-dimensional translational symmetry as follows:

$$f(\mathbf{r})=f(\mathbf{r}+\mathbf{s}_{mn}) \ , \qquad \mathbf{s}_{mn}=m\mathbf{s}_1+n\mathbf{s}_2 \ . \tag{A2}$$

The two vectors $\mathbf{s}_1$, $\mathbf{s}_2$ spanning the surface Bravais lattice, generate a 2×2 matrix S having $\mathbf{s}_1$, $\mathbf{s}_2$ as its rows. The surface Brillouin zone can be found from $G_\parallel$ given by

$$SG_\parallel^T=2\pi E \tag{A3}$$

because the rows $\mathbf{g}_1$, $\mathbf{g}_2$ of $G_\parallel$ span the surface Brillouin zone (E represents a 2×2 unit matrix). Hence,

$$\mathbf{g}_{pq}^\parallel=p\mathbf{g}_1+q\mathbf{g}_2 \tag{A4}$$

generates an arbitrary surface reciprocal-lattice vector. In this notation the two-dimensional Fourier transform of $f(\mathbf{r})$ becomes

$$f(\mathbf{r})=f(\mathbf{r}_\parallel,z)=\sum_{pq=-\infty}^{\infty}\tilde{f}(p,q,z)\exp(i\mathbf{g}_{pq}^\parallel\cdot\mathbf{r}) \ , \tag{A5a}$$

$$\tilde{f}(p,q,z)=\frac{1}{|\mathbf{s}_1\times\mathbf{s}_2|}\int_{1\mathrm{WS}_\parallel}d\mathbf{r}_\parallel' f(\mathbf{r}_\parallel',z)\exp(-i\mathbf{g}_{pq}^\parallel\cdot\mathbf{r}') \ , \qquad \mathbf{r}=(\mathbf{r}_\parallel,z) \ . \tag{A5b}$$

$|\mathbf{s}_1\times\mathbf{s}_2|$ is the area of the surface Wigner-Seitz cell ($1\mathrm{WS}_\parallel$) and enters the equations as the Jacobian $\mathrm{Det}(S^T)$ required by the integral transform yielding (A5). Next, one needs the two-dimensional Fourier transform of the three-dimensional spherical wave $f(\mathbf{r})=\exp(ik_0r)/r$. Its three-dimensional Fourier transform is

$$\tilde{f}(\mathbf{k})=\frac{1}{2\pi^2(k^2-k_0^2)} \ . \tag{A6}$$

To this result one applies the integral transform

$$\tilde{f}(\mathbf{k}_\parallel,z)=\int_{-\infty}^{\infty}dk_z\tilde{f}(\mathbf{k})e^{ik_zz} \ . \tag{A7}$$

In order to be able to use Cauchy's theorem, the result of this step has to be written as

$$\tilde{f}(\mathbf{k}_\parallel,z)=\frac{1}{2\pi^2}\lim_{\eta\to0}\int_{-\infty}^{\infty}dk_z\frac{e^{ik_zz}}{k_z^2-(k_{z0}+i\eta)^2} \ , \qquad k_{z0}=\sqrt{k_0^2-k_\parallel^2} \ . \tag{A8}$$

Extending the contour with a hemicircle and calculating residues is essentially easy, but (A8) introduces a moment of freedom as to the sign of k_z. For reasons of physics, choices will be made such that solutions always run away from the plane. This yields the required result as

$$\int_{-\infty}^{\infty}d\mathbf{r}_\parallel' e^{-i\mathbf{k}_\parallel\cdot\mathbf{r}'}\frac{\exp(ik_0r')}{r'}=2\pi i\frac{\exp(i|z|\sqrt{k_0^2-k_\parallel^2})}{\sqrt{k_0^2-k_\parallel^2}} \ . \tag{A9}$$

Equations (A5) and (A9) can solve, in general, interplanar scalar sums. We start by rewriting the real-space sum S

(A1) (omission of index j):

$$S(\mathbf{r},\mathbf{k}_0)=e^{i\mathbf{k}_0\cdot\mathbf{r}_\parallel}f(\mathbf{r}_\parallel,z)\ ,$$
$$f(\mathbf{r}_\parallel,z)=\sum_{mn}e^{-i\mathbf{k}_0\cdot(\mathbf{r}_\parallel-\mathbf{s}_{mn})}\frac{\exp(ik_0|\mathbf{r}-\mathbf{s}_{mn}|)}{|\mathbf{r}-\mathbf{s}_{mn}|}\ . \tag{A10}$$

The function $f(\mathbf{r}_\parallel,z)$ has exactly the two-dimensional translational symmetry as that required by (A5). Application of (A5) yields for the two-dimensional Fourier transform of $f(\mathbf{r}_\parallel,z)$

$$\tilde{f}(p,q,z)=\frac{1}{|\mathbf{s}_1\times\mathbf{s}_2|}\times\int_{1\mathrm{WS}_\parallel}d\mathbf{r}_\parallel\sum_{mn}e^{-i[\mathbf{k}_0(\mathbf{r}_\parallel-\mathbf{s}_{mn})+\mathbf{g}^\parallel_{pq}\mathbf{r}]}\times\frac{\exp(ik_0|\mathbf{r}-\mathbf{s}_{mn}|)}{|\mathbf{r}-\mathbf{s}_{mn}|}\ . \tag{A11}$$

Taking into account that from (A3) it follows that

$$\mathbf{g}^\parallel_{pq}\cdot\mathbf{s}_{kl}=2\pi Z\quad(Z\in\mathbf{Z})\ , \tag{A12}$$

Eq. (A11) can be written as

$$\tilde{f}(p,q,z)=\frac{1}{|\mathbf{s}_1\times\mathbf{s}_2|}\times\sum_{mn}\int_{1\mathrm{WS}_\parallel}d\mathbf{r}_\parallel e^{-i(\mathbf{k}_0+\mathbf{g}^\parallel_{pq})\cdot(\mathbf{r}_\parallel-\mathbf{s}_{mn})}\times\frac{\exp(ik_0|\mathbf{r}-\mathbf{s}_{mn}|)}{|\mathbf{r}-\mathbf{s}_{mn}|}\ . \tag{A13}$$

An elementary translation from $\mathbf{r}_\parallel-\mathbf{s}_{mn}$ to $\mathbf{r}_\parallel$, also known as the transposition rule, and a combination of the sum and the integrals over Wigner-Seitz cells at sites mn yields

$$\tilde{f}(p,q,z)=\frac{1}{|\mathbf{s}_1\times\mathbf{s}_2|}\int_{-\infty}^{\infty}d\mathbf{r}'_\parallel e^{-i(\mathbf{k}_0+\mathbf{g}^\parallel_{pq})\mathbf{r}'_\parallel}\frac{\exp(ik_0|\mathbf{r}'|)}{|\mathbf{r}'|}\ . \tag{A14}$$

Application of (A9) to (A14) yields a simple expression for $\tilde{f}(p,q,z)$. With that result one can return to Eq. (A5) and one arrives at the final general and elegant result:

$$S(\mathbf{r},\mathbf{k}_0)=\frac{2\pi i}{|\mathbf{s}_1\times\mathbf{s}_2|}\sum_{pq=-\infty}^{\infty}e^{i(\mathbf{k}_0+\mathbf{g}^\parallel_{pq})\mathbf{r}_\parallel}\frac{\exp(i\kappa_{pq}|z|)}{\kappa_{pq}}\ ,$$
$$\kappa_{pq}=\sqrt{k_0^2-(\mathbf{k}_{0\parallel}+\mathbf{g}^\parallel_{pq})^2}\ . \tag{A15}$$

Equation (A15) cannot be used if $z=0$ and is poorly convergent for $|z|\le a$. However, for $k_0\ll 2\pi/a$ and $z\to\infty$, only the 00 term of (A15) is required to find exact results. This is the optical limit and explains why (A15) is ideal for calculating the propagator. To verify the interrelationship between this derivation and the Litzman one, the following rule might be useful: *The surface reciprocal lattice belonging to a cleavage plane of a bulk crystalline solid coincides with the projection of the bulk reciprocal lattice onto that plane.* To obtain transfer tensors from Eq. (A15) requires application of the differential operator[20]

$$\overleftrightarrow{\mathbf{f}}_j(\mathbf{r})=a^3[\nabla\nabla^T+k^2\overleftrightarrow{\mathbf{1}}]S_j(\mathbf{r},\mathbf{k})\Big|_{\mathbf{r}=\mathbf{r}}\ . \tag{A16}$$

Application of this differential operator yields the expressions used in the main text and given in Eqs. (13), (14), (15), and (16).

APPENDIX B: PROJECTION PROPERTIES OF $\overleftrightarrow{\mathbf{d}}_{pq}$ [EQ. (15)]

From (A15) and (13c) it follows that

$$|\mathbf{k}_{pq}|=\sqrt{(\mathbf{k}_{0\parallel}+\mathbf{g}^\parallel_{pq})^2-\kappa^2_{pq}}=k\ . \tag{B1}$$

Using this relationship, it turns out that for the $\mathbf{d}_{pq}$, the following holds:

$$\mathbf{k}^T_{pq}\overleftrightarrow{\mathbf{d}}_{pq}\mathbf{x}\approx\mathbf{k}^T_{pq}[k^2\overleftrightarrow{\mathbf{1}}-\mathbf{k}_{pq}\mathbf{k}^T_{pq}]\mathbf{x}$$
$$=k^2\mathbf{k}^T_{pq}\mathbf{x}-k^2_{pq}\mathbf{k}^T_{pq}\mathbf{x}=0\ , \tag{B2}$$

independently from $\mathbf{x}$. As a result, the net effect of $\mathbf{d}_{pq}$ becomes projecting onto a plane perpendicular to $\mathbf{k}_{pq}$ of the vector $\mathbf{x}$ upon which it operates.

APPENDIX C: TWO-SLAB METHOD

The assumption is that the response of the wiggling zone can be incorporated into the traditional reflection and transmission coefficients. Hence, using a classical description, it is possible to isolate the separate coefficients in the following way. Figure 15 shows the configuration of this traditional model. The response of this slab will be calculated using Jones matrices and vectors. V refers to vacuum and M to medium, which should also explain the combinations. First we define D by

$$D=t_{VM}t_{MV}-r_{VM}r_{MV}\ . \tag{C1}$$

The Jones matrices for the front face, the interior, and the back face of the slab are given by the following expressions:

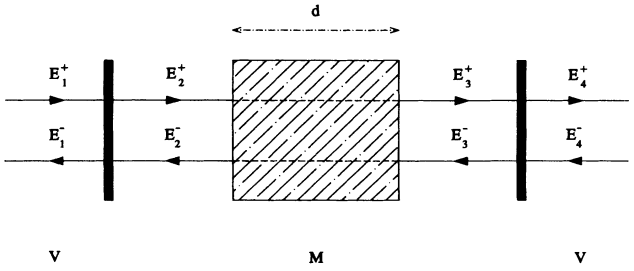

FIG. 15. Reflection-transmission from a slab using the Jones matrix description. V, vacuum; M, medium; d, slab thickness; $\mathbf{E}_i^+$, Jones vector forward propagating fields; $\mathbf{E}_i^-$; idem backward propagating fields; i, 1, 2, 3, 4.

$$\begin{vmatrix} E_1^+ \\ E_1^- \end{vmatrix} = \frac{1}{t_{VM}} \begin{vmatrix} 1 & -r_{MV} \\ r_{VM} & D \end{vmatrix} \begin{vmatrix} E_2^+ \\ E_2^- \end{vmatrix} , \tag{C2}$$

$$\begin{vmatrix} E_2^+ \\ E_2^- \end{vmatrix} = \begin{vmatrix} e^{-iqd} & 0 \\ 0 & e^{iqd} \end{vmatrix} \begin{vmatrix} E_3^+ \\ E_3^- \end{vmatrix} , \tag{C3}$$

$$\begin{vmatrix} E_3^+ \\ E_3^- \end{vmatrix} = \frac{1}{t_{MV}} \begin{vmatrix} 1 & -r_{VM} \\ r_{MV} & D \end{vmatrix} \begin{vmatrix} E_4^+ \\ E_4^- \end{vmatrix} . \tag{C4}$$

Those matrices contain no explicit angular dependence. For this reason, the final result will automatically include the angular dependency. Straightforward multiplication of the three matrices given in (C1)–(C3) yields the total Jones matrix for the slab. Using $E_4^- = 0$, one obtains the following expressions for the reflection coefficient r_{SLAB} and transmission coefficient t_{SLAB} of the slab:

$$r_{\mathrm{SLAB}} = \frac{E_1^-}{E_1^+} = \frac{r_{VM}\exp(-iqd) + D r_{MV}\exp(iqd)}{\exp(-iqd) - r_{MV}^2 \exp(iqd)} , \tag{C5a}$$

$$t_{\mathrm{SLAB}} = \frac{E_4^+}{E_1^+} = \frac{t_{VM} t_{MV}}{\exp(-iqd) - r_{MV}^2 \exp(iqd)} . \tag{C5b}$$

Substituting the value for D given in (C1) into (C5a) yields, after some elementary algebra, the following relationship:

$$r_{\mathrm{SLAB}} = r_{VM} + r_{MV} e^{iqd} t_{\mathrm{SLAB}} . \tag{C6}$$

Wijers and Del Sole[20] pointed out that (C6) yields the main TS equation (33). This derivation completes proof of the validity of (33) as concerns the angular dependency.

[1]T. E. Furtak and D. W. Lynch, Phys. Rev. Lett. **35**, 960 (1975).
[2]P. Chiaradia, A. Cricenti, A. Selci, and G. Chiarotti, Phys. Rev. Lett. **52**, 1145 (1984).
[3]K. C. Pandey, Phys. Rev. Lett. **47**, 1913 (1981); **49**, 223 (1982).
[4]N. Kar and A. Bagchi, Solid State Commun. **33**, 645 (1980).
[5]A. Bagchi, R. G. Barrera, and B. B. Dasgupta, Phys. Rev. Lett. **44**, 1475 (1980).
[6]A. Bagchi, R. G. Barrera, and R. Fuchs, Phys. Rev. B **25**, 7086 (1982).
[7]W. L. Mochán, R. Fuchs, and R. G. Barrera, Phys. Rev. B **27**, 771 (1983).
[8]W. L. Mochán and R. G. Barrera, Phys. Rev. Lett. **55**, 1192 (1985); Phys. Rev. B **32**, 4984 (1985); **32**, 4989 (1985).
[9]R. Del Sole and E. Fiorino, Phys. Rev. B **29**, 4631 (1984).
[10]A. Selloni and R. Del Sole, Surf. Sci. **168**, 35 (1986).
[11]R. Del Sole and A. Selloni, Phys. Rev. B **30**, 883 (1984); Solid State Commun. **50**, 825 (1984).
[12]R. Del Sole, W. L. Mochán, and R. G. Barrera, Phys. Rev. B **43**, 2136 (1991).
[13]D. E. Aspnes, J. Vac. Sci. Technol. B **3**, 1138 (1985); **3**, 1498 (1985).
[14]S. Selci, F. Ciccacci, A. Cricenti, A. C. Felici, C. Goletti, and P. Chiaradia, Solid State Commun. **62**, 833 (1987).
[15]V. L. Berkovits, L. F. Ivantsov, I. V. Makarenko, T. A. Minashvili, and V. I. Safarov, Fiz. Tekh. Poluprovodn. **21**, 433 (1987) [Sov. Phys. Semicond. **21**, 270 (1987)].
[16]V. L. Berkovits, I. V. Makarenko, T. A. Minashvili, and V. I. Safarov, Solid State Commun. **56**, 449 (1985).
[17]V. L. Berkovits, L. F. Ivantsov, I. V. Makarenko, T. A. Minashvili, and V. I. Safarov, Solid State Commun. **64**, 767 (1987).
[18]S. E. Acosta-Ortiz and A. Lastraz-Martínez, Phys. Rev. B **40**, 1426 (1989).
[19]C. M. J. Wijers and K. M. E. Emmett, Phys. Scr. **38**, 435 (1988).
[20]C. M. J. Wijers and R. Del Sole, Phys. Scr. T **25**, 325 (1989).
[21]G. P. M. Poppe and C. M. J. Wijers, Physica B **167**, 221 (1990).
[22]G. P. M. Poppe, H. Wormeester, A. Molenbroek, C. M. J. Wijers, and A. van Silfhout, Phys. Rev. B **43**, 12 122 (1991).
[23]C. M. J. Wijers and G. P. M. Poppe, Vacuum **41**, 624 (1990).
[24]C. M. J. Wijers, R. Del Sole, and F. Manghi, Phys. Rev. B **44**, 1825 (1991).
[25]G. P. M. Poppe, C. M. J. Wijers, and A. van Silfhout, Phys. Rev. B **44**, 7917 (1991).
[26]O. Litzman, Opt. Acta **25**, 509 (1978); **27**, 231 (1980).
[27]J. Grindlay, Physica **107A**, 471 (1981).
[28]W. L. Mochán and R. G. Barrera, J. Phys. (Paris) Colloq. **45**, C5-207 (1984).
[29]R. Del Sole, Mater. Sci. Eng. B **5**, 177 (1990).
[30]D. E. Aspnes, in *Proceedings of the 37th International Workshop on Electrodynamics of Interfaces and Composite Systems,* edited by R. G. Barrera and W.L. Mochán (World Scientific, Singapore, 1987).
[31]F. Manghi, R. Del Sole, A. Selloni, and E. Molinari, Phys. Rev. B **41**, 9935 (1990).
[32]R. Del Sole, W. L. Mochán, and R. G. Barrera, Phys. Rev. B **43**, 2136 (1991).
[33]J. Pastrnak and K. Vedam, Phys. Rev. B **3**, 2567 (1971).
[34]J. Vlieger, Physica **64**, 63 (1973).
[35]H. Wormeester, A. M. Molenbroek, C. M. J. Wijers, and A. van Silfhout, Surf. Sci. **260**, 31 (1992).
[36]P. P. Ewald, Ann. Phys. **49**, 117 (1916); **54**, 519 (1917); **54**, 557 (1917).